ELECTROCHEMICAL CHARACTERIZATION OF PbS QUANTUM DOTS CAPPED WITH OLEIC ACID AND PbS THIN FILMS – A COMPARATIVE STUDY

A.S. Cuharuc, L.L. Kulyuk, R.I. Lascova, A.A. Mitioglu, A.I. Dikusar

Institute of Applied Physics, Academy of Sciences of Moldova,
5 Academiei str., Chisinau, MD-2028, Republic of Moldova, dikusar@phys.asm.md

This research aims at probing electrochemical response of oleic acid capped PbS quantum dots deposited on a Pt electrode in 0.1 M aqueous sodium hydroxide solution by cyclic voltammetry and chronoamperometry. Quantum dots were also characterized by photoluminescence and IR spectroscopy. Cyclic voltammetry of bulk PbS thin films obtained via chemical bath deposition is investigated in order to interpret the data on PbS quantum dots. It was found that the two materials exhibit essentially similar voltammetric behavior; however, oxidation of PbS quantum dots tends to start at slightly more cathodic potentials than that of bulk PbS films. This effect is attributed to the influence of capping oleic acid that binds lead ions into an insoluble lead oleate thereby causing the cathodic shift of the formal redox potential. The procedures designed to partially remove oleic acid from PbS quantum dots result in the anodic shift of the PbS quantum dots oxidation towards the values characteristic for the bulk material. A possibility of determining absolute positions of conduction and valence bands in quantum dots by cyclic voltammetry is discussed but the influence of the energy level structure of PbS quantum dots on their voltammetric response was not revealed under the conditions of the present study. However, PbS quantum dots can withstand multiple redox cycles whereas bulk PbS films dissolve readily upon the first oxidation. The effect was attributed to the oleic acid layers on the PbS quantum dots surface, those layers preventing soluble oxidation products from diffusing into the bulk of solution. Certain PbS quantum dots samples showed remarkable stability against oxidation typical for PbS and starting at -0.2 V vs Ag/AgCl (sat.) and a stable response at oxidation and reduction at higher (0.55 V) and lower (-0.8 V) potentials, respectively.

УДК 544.6

INTRODUCTION

Semiconductor nanocrystals or quantum dots (QDs) exhibit electronic, optical, photochemical and photophysical properties greatly differing from those observed in corresponding bulk materials due to quantum size effects [1]. Transition metal chalcogenides are important semiconductor materials, especially on the nanoscale level because of their excellent photoelectron transformation properties and potential application in physics, chemistry, biology, materials science, etc. [2–7].

Among conventional semiconductors, PbS is particularly important because of its direct and narrow band gap (0.41 eV at 300 K), a large exciton Bohr radius of 20 nm, diverse morphologies [1] and almost equal effective masses of electrons, m_e^*, and holes, m_h^* [8]. The band gap blueshifts to the spectral region of 700–1500 nm (1.77–0.82 eV) upon the decrease in the nanocrystal diameter below the size of the excitonic Bohr radius due to quantum confinement effect. These properties of PbS quantum dots (Q-PbS) condition their use in a wide variety of photonic devices, electrochromic films, including light-emitting diodes [9, 3], infrared photodetectors [4–6] and photovoltaic devices [7].

The advantage of electrochemical studies of QDs consists in the fact that charge transfer events can be registered and characterized in terms of their energetics (peak potentials) and intensity (currents). The above mentioned advanced applications of QDs involve charge transfer to/from nanoparticles from/to a metal electrode or a conducting polymer or other environment. Hence a preliminary study of this phenomenon is needed.

There are numerous reports on investigation and probing semiconductor properties of various QDs by electrochemistry (see reviews [10, 11]). The absolute positions (that is, relative to the vacuum scale) of conduction and valence band edges as well as defect states are necessary for photovoltaic application wherein the match between the QD energy levels and those of the surrounding conducting polymers or other supports is crucial [12, 13]. Photoluminescence (PL) and absorption spectroscopy provide only the difference between the band edges whereas the absolute positions can be accessed by X-ray photoelectron spectroscopy (XPS) and the ultraviolet photoelectron spectroscopy [10]. However, the respective equipment is costly. Cyclic voltammetry (CV) offers a very tempting opportunity of measuring the absolute energy levels in semiconductor QDs as the experimental arrangement is very simple and the cost of equipment is not very high. Although all measurements were carried out with respect to a reference electrode, the absolute values can always be obtained from estimation of the potential of the normal hydrogen electrode with respect to the vacuum scale (-4.35 eV [14]) and, certainly, the potential of the reference electrode in use.

Many authors report on a successful correlation between QD energy levels determined by CV and their difference, the energy gap, found from absorption or PL measurements [10, 15–19]. In our opinion this correlation is not always unambiguous, possibly due to small ranges of QD sizes and/or insufficient amount of the sizes tested. Most probably, a very thorough and convincing investigation was performed by Inamdar with co-authors [18] wherein optical band gaps of Q-CdSe were compared with quasi-particle band gaps determined from the difference between the oxidation and reduction peaks corresponding to the valence and conduction bands of QDs, respectively.

Regardless of the fact whether the correlation between optical band gaps and electrochemical data are consistent or not, one thing is obvious from all the studies: the medium where measurements are performed critically affects the voltammetric response. Organic solvents are preferred due to their broad potential window available as compared to aqueous media; however, the use of ionic liquids with a phase transfer detergent accounts for very informative voltammograms, with band edges and defect states clearly defined (Q-CdSe in [10]).

In electrochemical experiments QDs are often prepared as a thin film on a working electrode. The conductivity of such a film may be very poor as large capping organic molecules that normally constitute the protective/passivating layer hinder charge transfer and, therefore, no useful data in voltammograms will be acquired as indicated by Guyot-Sionnest [20]. Those molecules can be substituted for shorter ones by simple immersion of a dried film into a solution of short-chain dithiols [21] or diamines and dithiols [22]. Such molecules serve as cross-links for nanocrystals, decreasing the distance between the nanocrystals.

In some cases cyclic voltammograms may not register charge transfer events in the form of peaks as is normally expected. A practically featureless voltammogram was acquired in [21] for Q-PbSe capped with 1,6-hexanedithiol. Nonetheless, the electron and hole injection into the QDs under study was clearly registered by changes in the IR absorption spectra during application of potential, and respective electron transitions were assigned to spectral bands. Therefore, electrochemical techniques alone may not be sufficient to track the events occurring in nanocrystals.

The reports devoted to electrochemical studies of Q-PbS are not very numerous [23–26, 13], with Chen's *et al*. work being probably the most cited [11, 23]. CV of Q-PbS of several sizes was presented in [13], where the authors demonstrated the shift of the reduction peak that correlated to the QD size, with larger particles being reduced at less negative potentials. However, a systematic study of voltammograms and electrochemistry of QDs was not done, probably because the CV analysis was not the main objective of the last cited research. Other researchers dealt with Q-PbS of only one certain size [23, 25, 26]; and if one compares the voltammograms presented therein, the qualitative difference will be found although the tested particles were of roughly the same size (3–4 nm). Reproducibility of voltammetric data was also a challenge in the present research as will be shown further.

Herein we report on CV of the synthesized Q-PbS capped with oleic acid (OA) and compare the acquired data with CV of the PbS film deposited onto a Pt electrode as a representative of the bulk material. A simple explanation of the voltammetric data is attempted based on the electrochemistry of semiconductors. The quantum confinement effect in the synthesized product is confirmed by PL spectra. We emphasize post-synthesis purification of Q-PbS and demonstrate its relevance for the voltammetric behaviour of the QD films. FT IR spectroscopy provides evidence on the structure of a QD as a core-shell system.

EXPERIMENTAL

Reagents. Lead (II) oxide (99.999%), oleic acid (OA, technical grade, > 90%), octadecene-1 (ODE, technical grade, > 90%), *bis*(trimethylsilyl)sulphur ($(TMS)_2S$) p.p.a., sodium citrate tribasic dehydrate (ACS reagent), lead (II) acetate trihydrate (puriss. p.a.) and thiourea (puriss.) were purchased form Aldrich and chloroform (HPLC grade), sodium hydroxide (puriss. p.a.), methanol (puriss. p.a.), sulfuric acid (puriss. p.a.) and acetone (puriss.) – from Riedel-de Häen and used without further purification. All aqueous solutions were prepared with triple-distilled water.

Synthesis and purification of Q-PbS. The synthesis procedure described below basically follows that in [27]. In a three-neck flask equipped with a thermometer, an inert gas supply tube and a magnetic bar, 0.49 g of PbO were combined with 5.0 g of OA under Ar atmosphere. The flask was heated and maintained at 150°C for 1 hour. These conditions allow removing some water formed as the reaction by-product. Afterwards, the flask was allowed to cool down to a certain temperature (indicated further in the text), depending on the desired size of the QDs in question, and the solution of $(TMS)_2S$ in ODE (0.22 g of $(TMS)_2S$ and 2.6 g of ODE) was injected into the flask with a syringe through a rubber septum, with the reaction mixture being intensively stirred. In 10 s an ice bath was placed under the flask to quench the reaction. The reaction products were dissolved in a minimum amount of chloroform.

Purification of the target product was performed via precipitation with methanol and re-dispersion in chloroform. Specifically, a quantity of methanol needed to cause the QDs coagulation was added to the chloroformic solution followed by centrifugation. The precipitate was separated, washed with methanol and re-dispersed in a minimum amount of chloroform. This cycle was repeated four times. It was noted that an increasingly larger amount of methanol was required to cause the precipitation. This procedure will be referred to in the main text as 'basic purification'.

Further purification is based on treatment with acetone and NaOH solution. Specifically, acetone was added to cloroformic solution of the QDs studied (4:1) to cause the coagulation and the mixture was refluxed under Ar atmosphere for ½ hour. The precipitate was removed by centrifugation and re-dispersed in chloroform and stored under Ar. The acetone extract being the purification by-product was preserved for IR analysis.

Then treatment in NaOH followed. Substitution of hexane for chloroform: from a certain amount of Q-PbS treated in acetone, chloroform was evaporated in vacuum and nanocrystals were re-dispersed in hexane since it is more volatile and does not react with NaOH. The solution in hexane was added to aqueous 0.5 M NaOH solution preheated to 50°C under Ar atmosphere. The mixture was gently stirred for 15 min, cooled down and centrifuged. The precipitate was thoroughly washed with acetone, dried and mixed with chloroform. The prepared product turned out insoluble in organic solvents, yielding unstable suspensions. The alkaline extract was acidified with diluted H_2SO_4, and the matter poorly soluble in aqueous medium was extracted twice with chloroform and preserved for the IR analysis. It will be referred to as 'chloroform extract' in the main text.

The sample notation given below indicates the synthesis temperature, and purification procedure and will be used throughout the text for Q-PbS designation prepared under various conditions.

prefix	synthesis temperature, °C	purification procedure	example
QD-	60, 100, 120	B – basic AC – in acetone SH – in sodium hydroxide	QD-120AC

Synthesis of lead (II) oleate. 0.4 g of PbO and 1.1 g of OA were mixed under inert atmosphere and kept at 150°C until all PbO dissolved. The reaction mixture was cooled down and dissolved in chloroform. Lead oleate was precipitated with methanol, filtered off, washed with methanol twice and dried at 60°C in a moderate vacuum.

Chemical bath deposition (CBD) of PbS films. In the synthesis procedure we largely departed from that in [28–30]. The deposited films demonstrate properties of the bulk lead sulphide. According to [30], from which we basically borrow the experimental parameters, the particle size in the deposits varied between 100–300 nm. The deposition time was not clearly revealed in that work; however, one can conclude that the authors carried out the deposition until the full completion of the reaction. Belova *et al.* [28] report that some 30 min suffice for lead (II) to quit the solution and deposit as PbS under the following conditions: pH = 12.5, citrate – 0.02 M, lead (II) – 0.005 M and T = 323 K.

In the present study, the solution prepared for the CBD was 0.025 M in sodium citrate, 0.01 M in lead acetate and 0.05 M in thiourea. By adding NaOH, pH was adjusted to 11–12. Then the solution was deaerated and thermostated at 50°C for ½ hour. The deposition started when thiourea was added to the solution of other components; at the same time, the Pt working electrode was immersed in the reaction medium. After 30–45 min a dark-grey mirror-like layer of PbS formed on the electrode that was further removed, thoroughly washed and transferred into the cell for electrochemical measurements with 0.1M NaOH deaerated beforehand.

Electrochemical measurements. A conventional one-compartment three-electrode cell connected to the potentiostat Parstat 2273 (Princeton Applied Research) was employed for the measurements. Pt wire electrodes served as working (apparent area – 0.063, true area – 0.108 cm^2, as determined by hydrogen adsorption [31]) and counter electrodes (apparent area 0.12 cm^2); Ag/AgCl/KCl (sat.) was used as a reference electrode. All the potentials cited in the present study are referred to this electrode unless otherwise stated. Potential sweeps reported herein were done at the rate of 25 mV/s unless otherwise stated. Both the cell made of Duran glass and electrodes were cleaned with hot sulphuric acid mixed with concentrated H_2O_2. The working electrode was finally cleaned by cycling potential between -0.2 and +1.2 V in 0.5M H_2SO_4 at 400 mV/s for 5 min, with the cycling always finished at the double layer region on Pt. The appearance of a tiny peak in the region of the oxidation of adsorbed hydrogen (voltammograms recorded at 50 mV/s), in addition to two other prominent peaks, served as the evidence of a very clean Pt surface [32].

Colloidal solutions or suspensions of Q-PbS in chloroform were drop-cast onto the working electrode to make up a noticeable layer and the solvent was evaporated in a moderate vacuum. Unfortunately, the amount of the solution dried on the wire electrode could not be determined or controlled due to the electrode shape. This circumstance did not allow a direct comparison of currents for different QD film depositions. All the measurements with QD films and bulk PbS were carried out in aqueous 0.1 M NaOH deaerated with Ar (4–7 L/h) for at least 30 min prior the experiment*.

IR measurements. IR spectra were acquired with the Perkin Elmer FT-IR spectrometer Spectrum-100. All samples (including the extracts just mentioned) were prepared as films on a KBr glass. Pure KBr glass was used for background measurement.

Photoluminescence measurements. PL measurements at room temperature were performed with a grating monochromator coupled to a cooled photomultiplier (PM) with S1 photocathode or to an InGaAs photodiode using standard lock-in detection techniques. The optical excitation was provided by the frequency-doubled YAG:Nd^{3+} laser (λ_{L2} = 532 nm).

RESULTS AND DISCUSSION

Photoluminescence. The PL spectra of PbS nanocrystals prepared at various synthesis temperatures are given in fig. 1. As is evident, PbS nanoparticles exhibit a bright band-edge luminescence spectra with clear exciton peaks at room temperature located in the near-IR spectral range. According to [33], these relatively narrow spectral bands are attributed to the radiative recombination of excitons in QD. The spectral PL maximum of PbS nanoparticles shifts from about 800 to 1300 nm as the synthesis temperature is increased, which indicates the growth of Q-PbS.

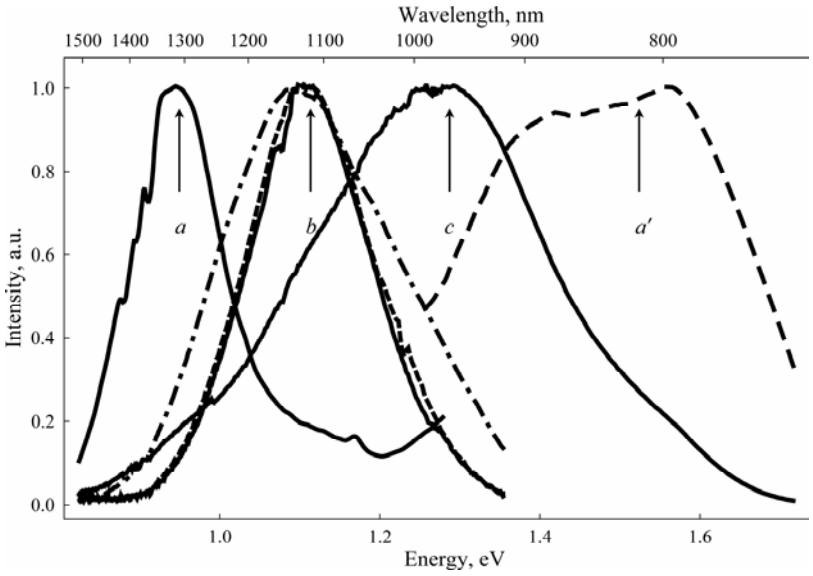

Fig. 1. Photoluminescence spectra of Q-PbS synthesized at different temperatures: a) at 120°C; a') the same sample as in a but recorded with the PM detector; b) at 100°C, the effect of purification procedure: basic purification (bold line), acetone treatment (dashed line) and NaOH treatment (dashed-dotted line); c) at 60°C

Assuming parabolic bands to the first approximation (the effective mass approximation) for a semiconductor nanocrystal with the radius R, the band gap energy, ΔE_g, due to quantization effects in the conduction and valence bands can be estimated through the theoretical equation derived by Wang [34]:

$$\Delta E_g = \left[E_g^2 + \left(\frac{2\hbar \cdot E_g}{m^*} \right) \left(\frac{\pi}{R} \right)^2 \right]^{1/2} \quad (1)$$

where R is in nm, E_g = 0.41 eV and $m^* = 0.089 m_e$ is the effective mass for PbS (m_e is an electron mass).

*In separate experiments, we established that this time is sufficient to diminish oxygen content by a factor of 30. Purging for longer times did not improve this value. The residual oxygen content in our experiments (ca. 0.2 mg/mL) was almost the same as reported in a special research [36]. PbS surface gradually oxidizes in the presence of dissolved oxygen; this conditions the OCP values of the electrode made of bulk PbS [37].

Formula includes the basic physical principles underlying the increase in the band gap when the nanocrystalline size decreases but is not quantitatively correct for dimensions smaller than 10 *nm*. Using the data from fig. 1, we estimated a nanocrsytalline radius of 4.4 nm, corresponding to $h\nu = 1.56$ eV, 5.5 nm for $h\nu = 1.29$ eV, 6.5 nm for $h\nu = 1.109$ eV and 7.8 nm for $h\nu = 0.95$ eV, respectively. According to the band gap energy rises for nanocrystals of smaller radii. However, it usually overestimates ΔE_g because the maximum of the PL spectra are shifted to lower energies relative to the absorption spectra – the shift known as Stokes shift [35]. An adjustable band gap of PbS opens a way to a new class of applications [9, 3–7].

IR spectroscopy. The study in this section was undertaken for three reasons. First, there was an idea that bulk material can be admixed to Q-PbS as a result of coagulation during purification procedure. Second, there was a hope to draw certain conclusions concerning the ligand state. Third, the present investigation provides proof for assumptions we initially made regarding the effect of the purification procedure.

Since bulk PbS band gap amounts to 0.41 eV [1], its absorption edge is expected to occur near 3300 cm^{-1}. However, the spectrum of the QDs studied (fig. 2) shows no edge absorption in that region, hence no bulk PbS is presented in the sample and the electrochemical signals to be discussed below are entirely due to Q-PbS.

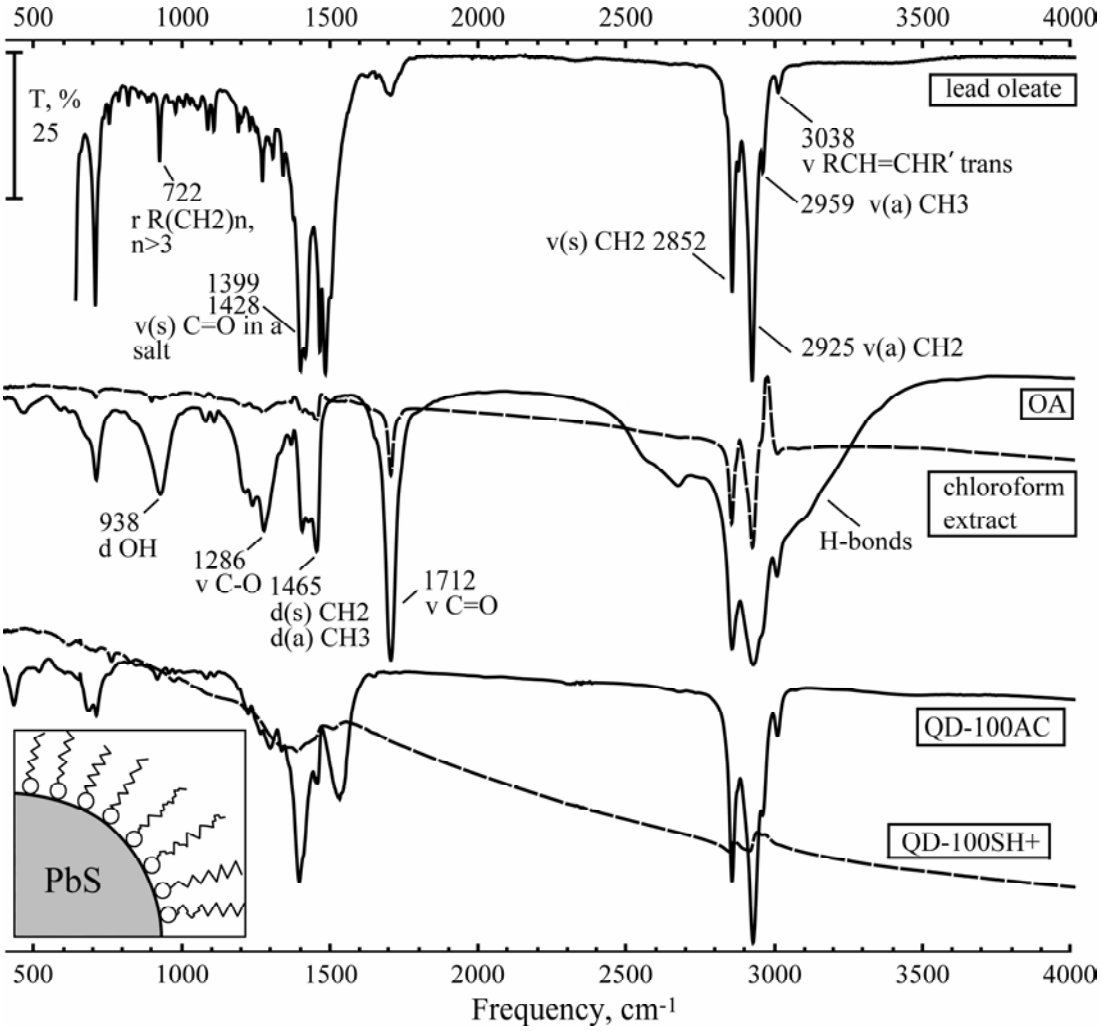

Fig. 2. IR transmission spectra of lead oleate, OA, the chloroform extract and two QD samples purified in acetone, QD-100AC, and in sodium hydroxide solution (enhanced treatment), QD-100SH+. The inset shows the proposed orientation of OA molecules on the PbS nanocrystal surface

The IR spectra of the QDs in our research can be easy understood by comparing them to the spectra of OA and lead oleate. Inspection of the region *ca.* 2800–3000 cm^{-1} reveals that the signal is due to the hydrocarbon chain of OA and virtually identical to that of lead oleate. It is of importance that the broad line presented in the spectrum of OA in the region 2400–3400 cm^{-1} caused by hydrogen bonding [38] (presumably in OA dimmers) is not observed in the QD and lead oleate spectra. Therefore, OA exists in the QDs investigated as a salt. Moreover, there are characteristic bands 1399 and 1428 cm^{-1} in the lead oleate spectrum, assigned to symmetrical valence vibrations of C=O bond of a carboxylic group anion in a salt, and these

bands are also strong in the QD spectrum. In fact, the QD spectrum essentially coincides with that of lead oleate, with some lines attenuated. Based on these data, we consider that the carboxylic group of OA faces the nanocrystal surface at the positions of lead atoms, thus forming a surface compound, lead oleate, and compensating "dangling" valence of surface lead atoms (see the inset in fig. 2). Such a conclusion was also made in [39] where Q-PbS capped with OA and TOPO were studied by XPS. Finally the signal (absorption edge) from PbS nanocrystals *per se* was not observed before 7800 cm^{-1} as expected for the synthesized QDs.

There are indications that ligands surrounding dissolved QDs are in a certain equilibrium with the solvent [20]. To make up a complete picture on that issue one would have to undertake a separate research. Here we can only qualitatively support the idea that underlies the purification procedure. Namely, the treatment of the QDs described in acetone and sodium hydroxide should reduce the amount of OA that either still drags after synthesis as an admixture or is chemically coordinated to the nanocrystal surface. The IR spectrum of the QD sample treated with acetone (Q-100AC) is presented in fig. 2 and was discussed above. The IR spectrum of the sample Q-100SH+, treated with NaOH as described in the Experimental section but at a larger concentration of NaOH and higher temperature, shows only very weak signals in the region of valence and deformation vibrations of the hydrocarbon tail. This suggests that the treatment with NaOH removes OA from the QDs, thus bringing them into a merger with each other. This can also be proved by the spectrum of chloroform extract (see Experimental) which albeit distorted is essentially that of OA (compare 'OA' and 'chloroform extract' traces in fig. 2). Practically the same spectrum was recorded for the acetone extract (not shown), hence the same matter was extracted by both NaOH and acetone, and it is OA or its sodium salt.

ELECTROCHEMISTRY

Generally, the electrochemical research we carried out revealed several aspects of Q-PbS electrochemistry in the conditions employed. Firstly, Q-PbS films show very similar response to that of the bulk PbS thin films, in terms of energetics of the reactions – peak potentials on voltammetric curves. Secondly, certain differences (again, compared to the bulk PbS film) in kinetics of the main oxidation peak (see A1 in fig. 3) have been established for certain QD samples. Thirdly, this oxidation peak diminishes gradually and surprisingly even increases during subsequent potential cycles for the QD samples whereas it drastically drops with every next cycle for the bulk PbS film. Fourthly, the oxidation and reduction peaks at the extremes of the potential range available emerge as very sharp and stable ones and appear independently of A1 for the QD samples only. The discussion of the experimental data for bulk PbS films and the QDs will be given further in two separate sections.

The question whether CV can provide absolute positions of band edges of Q-PbS was the main stimulus for the present research. We found out in the available literature that this question cannot be answered unequivocally. As mentioned in the Introduction, there are publications that demonstrated the power of CV for probing band edges and surface states of QDs (CdS [15], CdSe in [10, 16, 18]). Other authors report on the potential range of 1.7–1.8 eV in which Q-PbS gave no voltammetric signals in organic solvents, it being due to the band gap of Q-PbS, which was expected based on spectroscopic data [23, 25, 26]. The application of CV for HOMO and LUMO determination (ionization potential and electron affinity, as they are also referred to) in polymer molecules and conjugated organic compounds was reported by a number of authors. Some of them claim that absolute values of these energy levels and the band gap can be found from the positions of the first reduction (for LUMO) and oxidation (for HOMO) peak potentials [40–42] whereas other authors are more cautious in data interpretation [43, 44] or state that only a certain correlation between the oxidation and reduction peaks, on one hand, and HOMO and LUMO, on the other hand, can be claimed [45, 46].

Bulk PbS film electrochemistry. We are convinced that electrochemistry of bulk PbS film will serve a basis for understanding phenomena in Q-PbS. Fig. 3 schematically depicts the cyclic voltammogram of a PbS thin film, which was composed of the data from multiple experiments so as to make a whole picture of this very complex process. Any real voltammogram would miss some of the peaks since the signals are either very weak relative to other ones or undetectable at all. The reliability of this scheme is based on the fact that each peak was registered 3–11 times, and table 1 provides some statistical data and comments for every peak. The picture also reflects the right succession of peaks during potential sweep starting from the open circuit potential (OCP) in the cathodic direction.

To ensure that the peaks in question are all related to PbS electrochemistry, we provide the cyclic voltammogram of the blank: a pure polycrystalline Pt electrode in deaerated 0.1M NaOH (fig. 3, left inset). The voltammogram is very similar to the one reported in [47], featuring reductive hydrogen adsorption in the far cathodic region, the formation of platinum oxide commencing at -0.2 V and reduction of the oxide on the reverse scan with the peak potential at -0.2 V. In the present study, the platinum oxide formation and reduc-

tion are important as they appear in the voltammograms of the QD films and bulk PbS thin films usually at later cycles when Pt surface becomes exposed (see below).

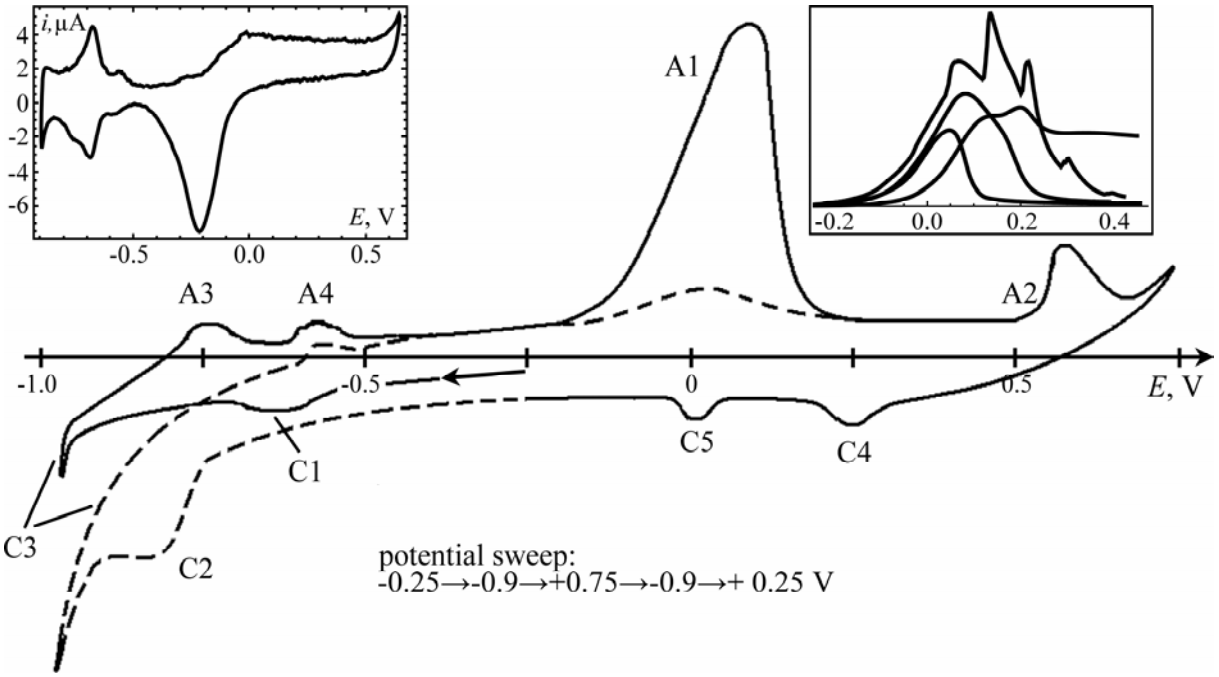

Fig. 3. Schematic presentation of cyclic voltammograms of studied bulk PbS thin films. Potential sweep starts from -0.25 V (usual location of OCP) and then follows the direction given in the figure. The dashed line is the initial part of the second cycle. The right inset shows the diversity of real experimental profiles of peak A1 and the left one – the cyclic voltammogram of polycrystalline Pt in 0.1M NaOH

Table 1. Voltammetric signals of bulk PbS thin films

peak	peak potential, V	comments
C1	-0.64 – -0.44	weak signal (~1 μA) detected during cathodic excursions of potential, not detected after anodic one
C2	-0.81±0.02	detected only after anodic excursion, rather strong (25 μA)
C3 (wave)	starts at -0.7 – -0.6	not a peak but a rising cathodic current becoming much stronger after anodic sweep
C4	0.20±0.04	always detected, currents 1–20 μA
C5	0.04±0.03	very weak and rarely detectable
A1	0.00 – 0.11	always detected, diverse in shapes, 140–400 μA during first cycle
A2	0.57±0.02	detected very frequently , currents 8–80 μA
A3	-0.77 – -0.48	weak peaks (< ≈1 μA), observed frequently and frequently together,
A4	-0.65 – -0.37	i.e., sometimes only one of them detected

Peak C1appeares in all voltammograms as a very weak and broad signal and can be assigned to the reduction of oxidized PbS surface, i.e., elemental sulphur (during the synthesis procedure we minimized exposure of PbS to the atmosphere but it could not be completely eliminated). In [48], galena (natural PbS) was exposed to oxygen-saturated alkaline solution for different times and a broad peak was observed during the cathodic sweep between ~ -0.9 – -0.4 V vs Ag/AgCl (sat), depending on the time of exposure, and it was attributed to the reduction of S^0 on the electrode surface. A similar peak near -0.5 V vs SCE was also observed in the deoxygenated alkaline solution during the cathodic sweep on galena electrode following brief oxidation of it by excursion of potential in the anodic direction [37].

Reduction of PbS depends on pH and commences at about -1.2 V vs SCE in 0.1 M NaOH [49, 50], shifting in the anodic direction, with decreasing pH. The cathodic wave C3, as we observed, does not really fit these data, starting at appreciably more anodic potentials; however, the overall picture in the cathodic region may suggest that nevertheless the reduction takes place. Specifically, in [37] and [51] the anodic wave ~-0.65 V vs SCE was observed after a sweep reversal to the anodic direction. Our voltammograms also possess this peak, A3, and frequently another peak A4 can be observed in that region of potentials. Saloniemi *et al.* assigned the anodic wave to the dissolution of elemental lead previously deposited on PbS [51]. Hence

it can be concluded that C3 represents PbS reduction, yielding Pb^0 and SH^-. As for this signal C2 after a far anodic excursion (see dashed line of the second cycle in fig. 3), it is not only reduction of PbS; starting at ~ -0.6 V, it largely represents the reduction of matter generated by electrochemical PbS oxidation. The importance of processes in this potential range for PbS restoration will be discussed later.

The most prominent feature of PbS electrochemistry is the anodic peak A1. According to the available literature, in strong alkaline medium (pH ≥ 13), there should be not a peak but a monotonously increasing signal starting at ca. -0.2 V vs SCE. Formation of soluble products that are not deposited on the electrode surface accounts for the absence of a peak or pre-peak [48, 52]; at a lower, but not acidic pH, partial passivation of the surface occurs due to the formation of S^0 and PbO [48]. High pH values favour the formation of plumbite ions; and increasingly large amounts of thiosulfate along with S^0 are also formed as Gardener and Woods argue [48]. According to their calculations, nearly 60% of PbS yield S^0 and 40% – $S_2O_3^{2-}$ at pH = 13. Hence we can write down main oxidation reactions as follows:

$$PbS + 3OH^- - 2e \rightarrow HPbO_2^- + H_2O + S,\ E_1^0, \tag{2}$$

$$2PbS + 12OH^- - 8e \rightarrow 2HPbO_2^- + S_2O_3^{2-} + 5H_2O,\ E_2^0. \tag{3}$$

The formal potential, $E^{0\prime}{}_1$, at pH = 13 for reaction can be calculated based on the value $E^0{}_3$ reported in [48] for reaction (4)

$$PbS - 2e \rightarrow Pb^{2+}(aq) + S, \quad E_3^0 = +0.1\ \text{V vs SCE} \tag{4}$$

$$E_1^{0'} = E_3^0 + 0.827 - 0.0885\ \text{pH}$$

thus giving $E^{0\prime}{}_1$ = -0.22 V vs SCE (a shift of -0.32 V), which is consistent with the initial potentials reported [48, 52] and confirmed in the present study (-0.25 – -0.20 V). We should stress that the formal potential can become close to the initial one, being always less than E_{max}, if the constant, k_0, in Batler-Volmer equation is sufficiently small, which is generally true for irreversible redox reactions and therefore is justified for use in our argumentation*.

It can be demonstrated that the formal potential, $E^{0\prime}{}_2$, of reaction shifts from its standard potential, $E^0{}_2$ = 0.614 V vs SHE [48], by -0.96 V at pH = 13, so that $E^{0\prime}{}_2$ = -0.346 V vs SHE or ~ -0.57 V vs Ag/AgCl (sat). Therefore reaction (3) is thermodynamically even more favourable than reaction (2). Nonetheless, the experiment is consistent with reaction (2), which can be attributed to the kinetic hindrance of reaction (3).

Our findings show that oxidation of PbS is more complex than it can seem and reactions (2) and (3) are not completely consistent with experimental observations. We have to acknowledge the formation of insoluble lead species on the fact that oxidation peak A1 and most of other peaks resume in the second and subsequent cycles, with the magnitude largely reducing with every next cycle. Restoration of PbS electrochemistry after the first cycle is possible only if a part of both sulphur and lead species are deposited on the electrode surface. No doubt, a significant portion of lead sulphide dissolves during oxidation and diffuses into the bulk of solution. A specially designed experiment showed that PbS restores from *adsorbed* species at potentials < ~ -0.6 V but not from those surrounding the electrode as one might think. Freshly prepared bulk PbS film underwent the potential cycle -0.4 → +0.75 → -0.4 → +0.75 V (fig. 4,*a*). Oxidation peak A1 appeared, as expected, during the first sweep but not during the second one, thus suggesting that re-formation of PbS occurs at more negative potentials. The next cycle, +0.75 → -0.9 → +0.75 V, was accompanied by bubbling Ar through the solution (fig. 4,*b*). We did not observe any distortions on a voltammetric curve due to uneven stirring, and PbS oxidation was observed again; hence, only adsorbed species participate in all the processes involved. Taking into account the literature just discussed, we propose another reaction for the oxidation process, which simply states that only a part of lead diffuses away as $HPbO_2^-$ and the other part is PbO deposited on the electrode:

$$PbS + 2OH^- - 2e \rightarrow PbO + H_2O + S. \tag{5}$$

The fact that we observed a peak rather than a monotonously rising current can be explained by two factors: 1) a limited amount of PbS thin film available on the electrode (unlike the cases when the working

*See e.g. the work by Hubbard [58] that is discussed below in more detail.

electrode was made of massive PbS piece and, hence, the matter was quasi-infinite); 2) the PbS surface is being passivated. These two factors do not exclude each other and can operate simultaneously. Further, the peak, as it is depicted in the scheme, is not always observed; instead, it can be either broader, or lose the peak shape at all, or appear as multiple successive peaks (see the right inset in fig. 3). It was noticed that processes with higher currents tend to deviate from the "ideal" shape depicted and shift anodically. One can assume that this is conditioned by the shift of $E^0{}'_1$ due to its dependency on pH. When reaction (2) proceeds it consumes 3 moles of OH^- per each mole of PbS. while reaction (3) – 12 moles of OH^-, resulting in a decrease of pH near the electrode and, as a consequence, the anodic shift of $E^0{}'_1$. Further we will discuss some kinetics aspects of process A1.

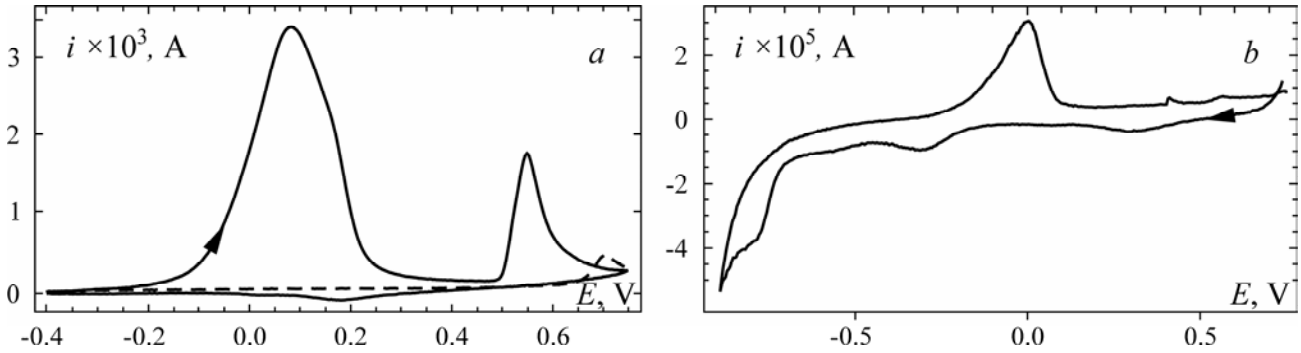

Fig. 4. Cyclic voltammograms of freshly prepared bulk PbS thin film. (a) Potential sweep -0.4 → 0.75 → -0.4 → 0.75. Continuous curve shows the first cycle. (b) Potential sweep 0.75 → -0.9 → 0.75 followed after the sweep given in (a) and accompanied by stirring the cell solution with argon

The reasons behind the distortion of the peak A1 shape are beyond our comprehension at the moment but simpler cases when process A1 is represented as a single "ideal" peak can be characterized to some extent. Several experimental facts have been established and summarized in table 2 and fig. 5. In the table, the Tafel-type linearization data for peaks A1 are presented and in the Appendix we substantiate how potentiodynamic curves can be used to obtain the Tafel constant for adsorbed species. As is evident, the Tafel constants vary in a narrow range, corresponding to the Tafel slopes 104–126 mV/decade. Furthermore peak current-to-charge ratio is constant q/i_{max} = 5.32 (see fig. 5,*b*) for all the data. This suggests that the processes represented by the "ideal" peak shape are essentially the same in terms of their nature and kinetics. The differing peak currents are *only due to the amount of PbS available*. Peak potentials vary in the range 0–0.11 V, with the majority of data confined to 0.04–0.08 V. There is no correlation between peak potentials and peak charges or currents; therefore peak potentials are not conditioned by the amount of PbS reacted or its kinetics and depend on an unknown factor. This implies that, unfortunately, the bulk PbS film oxidation cannot be characterized by a certain peak potential.

Table 2. The data on the linearization of peak A1 for the bulk PbS films and peak A1 potentials

cycle number*	intercept	slope	slope, mV/decade	E_{max}, V
c2	3.52	8.63	116	0.041
c3	-4.22	7.91	126	0.044
c1	-3.63	8.36	120	0.049
c2	-4.37	9.49	105	0.11
c4	-4.39	9.65	104	0.067
c5	-4.53	9.08	110	0.054
c2	-4.21	8.61	116	0.0252

**) for a given bulk PbS film, several potential cycles were carried out and are indicated. The curly brackets unite the cycles of the same film.*

The Tafel linearization mentioned above is presented in fig. 5,*a*. Deviations from the linear behaviour are characteristic and always observed in the post-maximum region. This can be regarded as an "intervention" of another process that results in a significant decrease of the rate of PbS oxidation, which can be due to the passivation of PbS surface, but not to limited amounts of PbS on the electrode. The oxidative dis-

solution of PbS can be interpreted in terms of dissolution of a binary bivalent ionic semiconducting compound and described by ion transport kinetics [14]:

$$\text{BLP} \quad i = 2ek_S^+ A\left[\text{S}\right]^* p_b^2 \exp\left[\frac{2e\Delta\phi_{SC}}{kT}\right], \tag{6}$$

$$\text{FLP} \quad i = 2ek_{\text{Pb}}^+ A\left[\text{Pb}\right]^* \exp\left[\frac{\alpha_{\text{Pb}}^+ e\Delta\phi_{\text{H}}}{kT}\right] \tag{7}$$

where i is current, e is elemental charge, p_b is bulk concentration of holes, k is the Boltzmann constant, T is absolute temperature, k_s^+ and k_{Pb}^+ are rate constants, $[\text{S}]^*$ and $[\text{Pb}]^*$ are surface concentrations of sulphur and lead ions; A is the electrode area, α_{Pb}^+ is the transfer coefficient of lead ions, $\Delta\phi_{SC}$ and $\Delta\phi_{\text{H}}$ are potential drops across a semiconductor space charge layer and the Helmholtz layer, respectively. Formulas (6) and (7) apply when the band edge level pinning (BLP) or the Fermi level pinning (FLP) take place, respectively. The Tafel slope for BLP, implied in (6), at 298 K, is 30 mV/decade, which is not consistent with our data that show 114 mV/decade, on average. Therefore dissolution occurs with FLP – the change of potential drop applied is entirely in the Helmholtz layer – and the transfer coefficient is $\alpha_{\text{Pb}}^+ = 0.52$. The Tafel slopes of 57–76 mV/decade were reported in [53] for galena dissolution in acidic medium, higher values related to surface states of the galena samples.

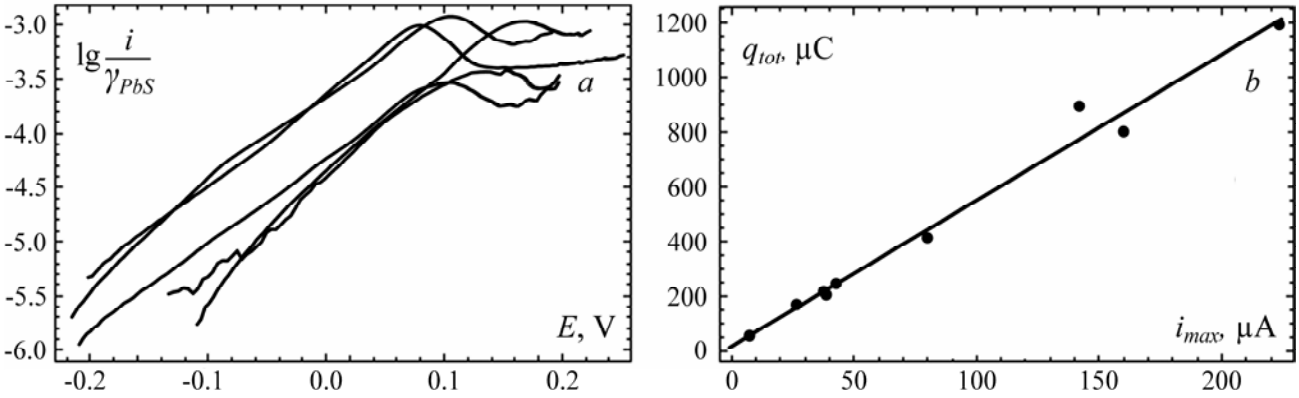

Fig. 5. Linearization of peak A1 for the bulk PbS films (a) and the plot of total peak charge vs peak current (b)

Next, we attempt to present basic redox reactions of the bulk PbS film from the standpoint of semiconductor electrochemistry. Richardson and O'Dell found a polarizable space charge layer of their galena samples in the potential range *ca.* -0.6 – -0.2 V vs SCE with the flat-band potential close to -0.6 V or -0.2 V for highly n- or p-type samples, respectively [37]. Therefore one can admit that these potentials determine the positions of conduction (CB) and valence bands (VB) of PbS. High anodic currents observed for our samples in the present study suggest that they are of p-type and the Fermi level in PbS, $\varepsilon_{F(SC)}$, is located close to VB (fig. 6,*a*). Our experiments also showed that anodic polarization from OCP immediately results in the anodic current of peak A1. This implies that the Fermi level in PbS becomes lower than the redox Fermi level, $\varepsilon_{F(dec,\ p)}$, corresponding to p-type decomposition of PbS – a thermodynamic condition for oxidative decomposition of a semiconductor [14, 54]:

$$\varepsilon_{F(SC)} < \varepsilon_{F(dec,p)} \tag{8}$$

or in terms of potentials on electrochemical scale

$$E_{F(SC)} > E_{F(dec,p)}. \tag{9}$$

Indeed, if $E_{VB} \sim$ -0.2V and $E_{F(dec,\ p)} = E^{0\prime}{}_1 =$ -0.22 V, then condition (9) is met in p-type PbS as soon as the electrode is polarized anodically, $+e\eta$ (fig. 6,*b* and *d*).

Under cathodic polarization, $\varepsilon_{F(SC)}$ moves cathodically, $-e\eta$, charging surface states, SS, corresponding to the oxidized PbS surface as discussed above, and when conditions (10) and (11) are met

$$\varepsilon_{F(SC)} > \varepsilon_{F(dec,n)} \tag{10}$$

$$E_{F(SC)} < E_{F(dec,n)} \tag{11}$$

PbS undergoes reductive decomposition (fig. 6,*c* and *d*), if we accept that $E_{F(dec,\ n)}$ is ~ -1.2 V as established in publications cited above. As is evident, the band gap and absolute positions of VB and CB are not involved in this process; conditions (8)–(11) result only from thermodynamic reasons and are not related to the structure of energy levels.

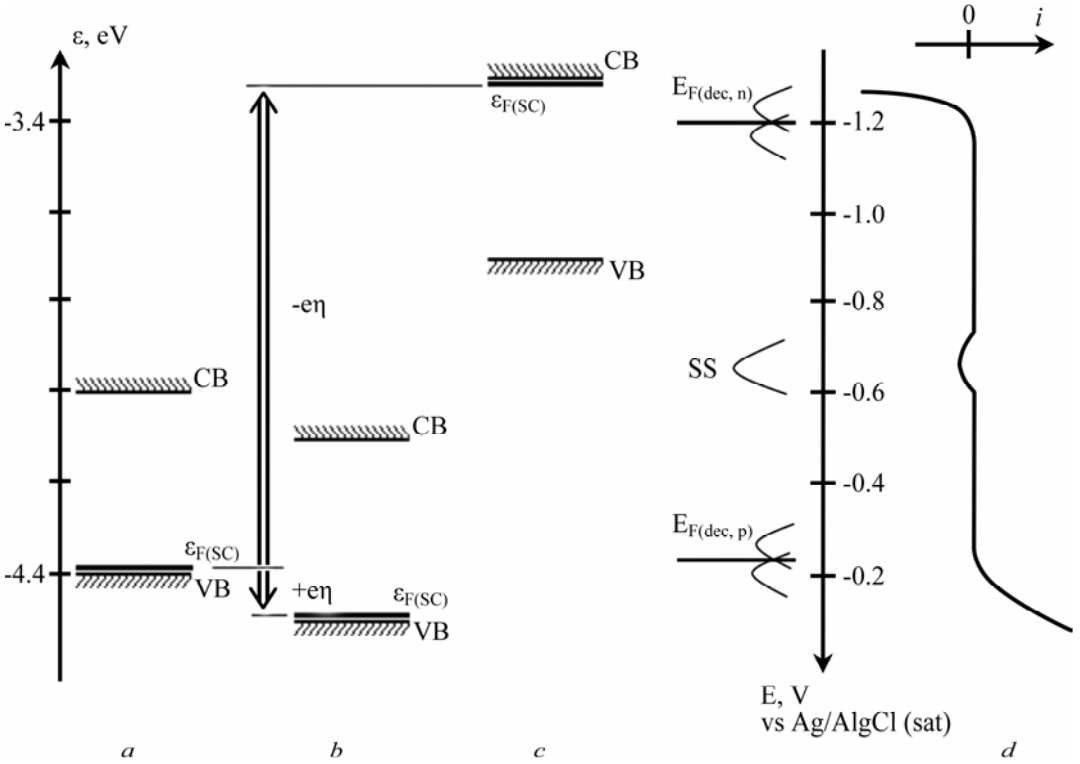

Fig. 6. Energy levels of bulk PbS films under OCP (a), anodic polarization (b), cathodic polarization (c). Schematic presentation of the respective i-E profile, redox Fermi levels of oxidative, $E_{F(dec,\ p)}$, and reductive $E_{F(dec,\ n)}$ decomposition of PbS and surface states, SS (d). (Note that in this schematic picture, the bands are not depicted curved for simplicity.)

As for other peaks, C4 and C5, the nature of reactions involved has not been clarified in the present study; however, they will be mentioned in the following section.

Electrochemistry of Q-PbS. The first important aspect of Q-PbS electrochemistry under the conditions of study consists in proximity of redox reaction potentials of Q-PbS samples and of bulk PbS thin films. fig. 7,*a* demonstrates 15 consecutive cycles of potential for the sample QD-120AC. Most of the peaks detected for a bulk PbS film appear in this voltammogram as well. Note that the cathodic peak at -0.3 – -0.2 V on this and other voltammograms represents reduction of Pt oxide formed during the anodic potential excursion beyond -0.1 V. Peak potentials for reactions denoted A2, C4 and C5 on the first cycle are 0.598, 0.209 and 0.063 V, respectively. These values fit (within the standard deviation (s.d.)) those presented in table 1 for the same redox reactions of a bulk PbS film. In the second cycle, process A2 is presented by an additional peak at 0.52 V. The cathodic reaction C3 appears as a rather well-defined peak unlike the wave observed for a bulk PbS film. Peak A1 is shifted towards negative potentials; it is highly reproducible with an average value -0.05 V. If compared to peak potentials for bulk PbS films, one can conclude that *Q-PbS undergoes oxidation easier*. However, most remarkable features of oxidation that make the difference between the two materials are 1) gradual decrease of peak currents during cycling, 2) temporal upsurge of peak currents during cycling, and 3) unexpected reproducibility of peak currents both within a given experiment and between replicate experiments.

A gradual decrease of peaks A1 in subsequent cycles is characteristic of the QD samples only. We assume that OA forms “a bag” surrounding nanocrystals, hence preventing soluble oxidation products from diffusing into the bulk of solution. Alternatively, lead oleate rather than plumbite can be admitted as one of

the oxidation products; this compound is insoluble in an aqueous medium and keeps lead ions available for the following reaction with S^{2-} forming during the cathodic potential sweep.

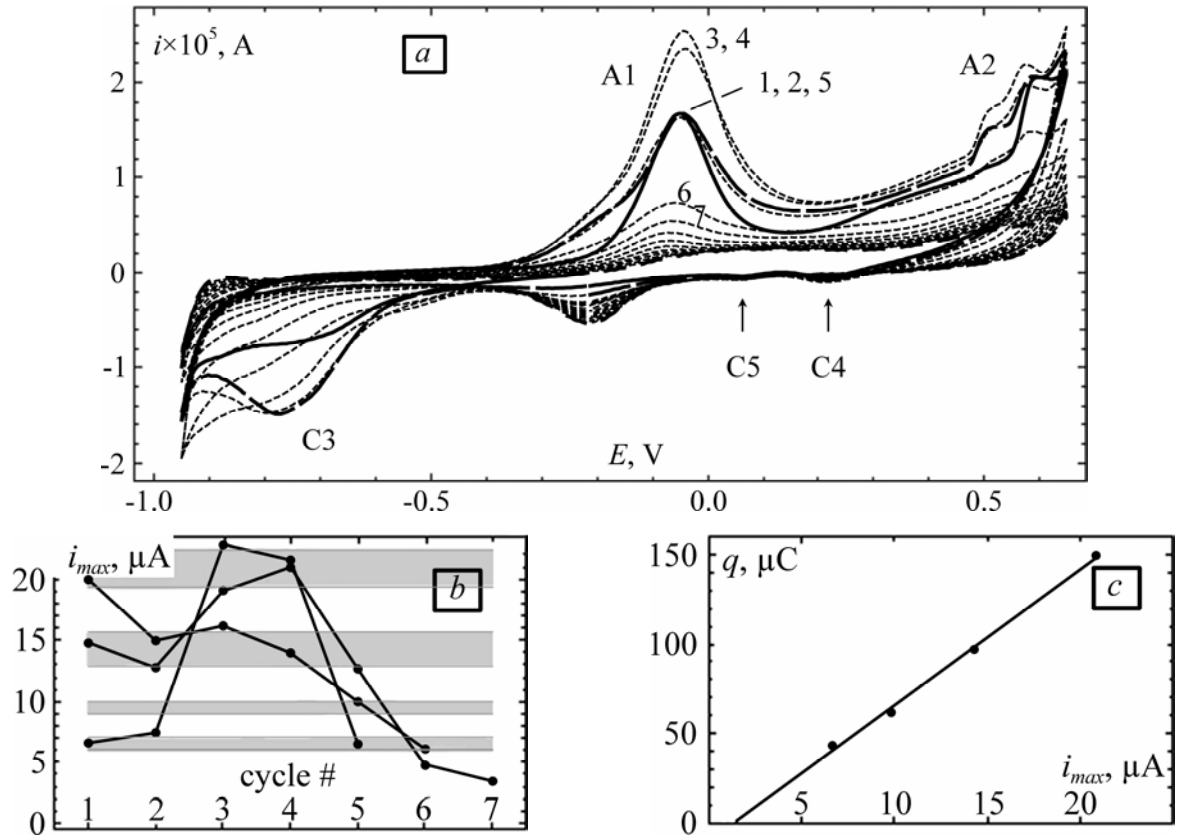

Fig. 7. (a) Cyclic voltammograms of QD-120AC: cycle 1 (bold continuous line), cycle 2 (bold dashed line), cycles 3 – 15 (thin short-dashed line). The first seven cycles are marked with numbers. (b) The plot of peak A1 currents vs cycle number. (c) The plot of group mean peak A1 charge vs group mean peak A1 current

In fig. 7,*a*, peaks A1 of the first 7 cycles are marked with numbers to show the effect just mentioned. Under the conditions of the present study, one cannot deposit a reproducible amount of Q-PbS on the electrode, hence, peak currents are expected to be different with every new deposition of Q-PbS. However, the values that peak currents assumed, although vary, form four groups or clusters[*]. Fig. 7,*b* exemplifies how peak currents change with a number of cycles for three different PbS depositions. The gray bands show limits for every current group as mean± s.d. Peak charges also follow grouping which is not so pronounced as that of currents[**]. The hierarchical analysis yields three clusters instead of four, with the charge values corresponding to the two first current groups being merged into one. Yet, if one sets to find four clusters and plots the group mean values for the charges versus group mean values for the currents, a straight line results with the slope (q/i_{max} ratio) equal to 7.56 (fig. 7,*c*). This quantity is smaller for a bulk PbS film (q/i_{max} = 5.31) possibly because Q-PbS gives a rather symmetric peak A1. Kinetics of oxidation is quite similar to that established for a bulk PbS film. Specifically, if one attempts to linearize *i-E* profile in a manner given above, the resulting line is generally not straight. The Tafel slopes for the data demonstrating a reasonably linear behaviour are within 100–115 mV/decade.

The explanation of unusual reproducibility of peak currents, that we propose, consists in layer-by-layer dissolution of Q-PbS. Apparently, a certain integer number of layers reacts during the potential sweep. It is not possible to count the number of layers precisely based on the peak charge as the true area of Q-PbS coating and packing density of nanocrystals in the layers are unknown. To the first approximation, one can estimate that thickness of the PbS layer corresponding to the first charge group (average 43 μC) is about 0.65 nm, which is close to the lattice constant of galena 5.936 Å [55], assuming that Q-PbS layer has the same area as the true electrode area.

[*] Hierarchical clustering of data (20 values) was performed by means Mathematica and Silhouette statistics was employed for the significance test.

[**] The peak charges undergo greater dispersion since they are more sensitive to baseline subtraction than peak currents. In the case of Q-PbS, baseline for peak A1 cannot be taken as a straight line thus making peak treatment less accurate.

The cathodic shift of oxidation peak A1 can be explained by the change in the formal potential of reaction (2), E^0_1', in alkaline media since equilibrium concentration [Pb^{2+}] decreases due to the formation of $HPbO_2^-$. In the case of Q-PbS, OA plays a role of a ligand, additionally decreasing [Pb^{2+}] and thereby moving E^0_1' further in the cathodic region. Unfortunately, the data on the solubility product of lead oleate are not available in literature to date, thus it is not possible to provide quantitative basis for this supposition. *The given explanation implies that the size of nanocrystals does not affect their redox properties*. More experimental evidences will follow later in the text in support of this idea.

The effect of the developed purification procedure can be appreciated from voltammograms of the sample QD-100 that underwent basic purification with methanol and chloroform (fig. 8,*a*), further treatment in acetone (fig. 8,*b*) and further treatment in the sodium hydroxide solution (fig. 8,*c*). The reduction of noise and qualitative improvement of voltammetric response can be seen on the *i-E* profiles of the samples of higher purity. Since in purification OA is removed, as discussed in the 'IR spectroscopy' section, one can infer that excessive OA imposes insulating properties on the QD layers.

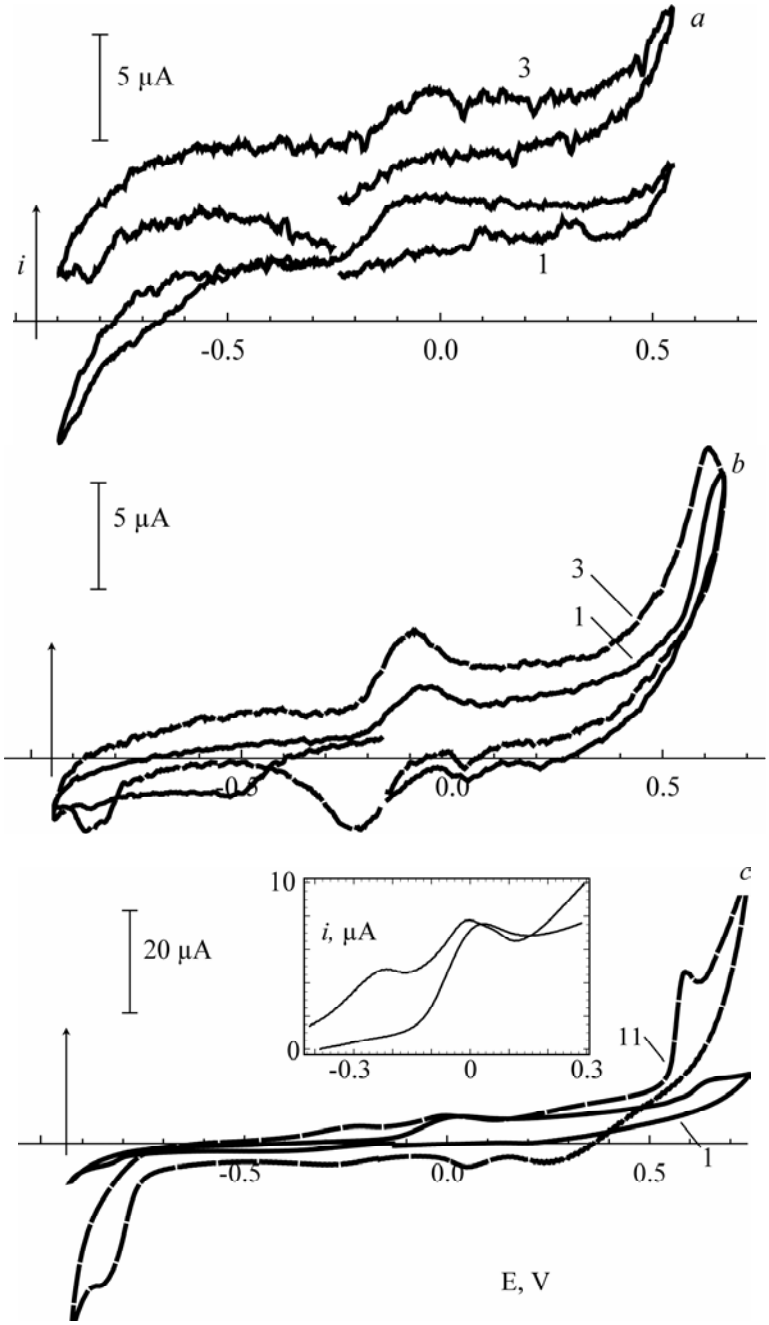

Fig. 8. The effect of purification procedure on the voltammetric response of the QD samples. (a) Sample QD-100B obtained with only basic purification procedure; (b) QD-100AC – after additional acetone treatment; (c) QD-100SH – after additional treatment in NaOH. The numbers indicate potential cycle sequence number for a given deposition. The inset shows anodic currents in the region -0.4 – 0.3 V for sample QD-100SH

Fig. 8 also demonstrates that peak potential, E_{max}, for peak A1, depends on the environment, i.e., amount of capping OA. For the sample purified in acetone, E_{max} ~ -0.08 V whereas for the sample treated in NaOH, it is *ca.* 0.02 V. The PbS nanocrystals were not significantly affected by this treatment since the PL maximum did not change (see curves *b* in fig. 1). Another confirmation of the environment effect on the peak potential was obtained through an experiment with samples QD-60B, which yielded two anodic peaks E_{max} = -0.22 and -0.02 V; after the treatment in acetone, a single peak appeared at ~0.02 V; an enhanced treatment in NaOH (0.5 M NaOH and 100°C) yielded a sample (QD60-SH+, see its IR spectrum in fig. 2) with a very pronounced peak A1 with E_{max} = 0.05 V, which is very close to E_{max} , typically observed for bulk PbS (data not presented). It is worth noting that PL spectrum for QD60-SH+ differs significantly from that of QD-60B and QD60-AC: the PL maximum (1250 nm) is red shifted by 200 nm and the peak is very broad, which is indicative of partial merging of nanocrystals. Yet the quantum confinement effect was still there. *All said above signifies that the quantum confinement effect and, therefore, energy structure of PbS are not manifested in these experiments*. As mentioned in the Introduction, the medium in which measurements are carried out critically affects the voltammetric response. Therefore we do not generalize this conclusion and admit that the use of a different medium might yield more informative voltammograms of Q-PbS.

The QD samples studied by us show certain irreproducibility between each other. On the one hand, the sample QD-120AC has a pronounced oxidation peak A1 with its unusual properties discussed earlier. On the other hand, the samples QD-100AC and QD-60AC show a very moderate peak A1 or the absence of that. Removing much of OA from QD-60AC gives an intensive peak A1 which, although decreased gradually during potential cycling as expected for QDs, does not result in a temporal increase of the peak current. Apparently, the amount of OA has a very subtle effect on the electrochemical response of the QDs investigated besides the shift of E_{max}, and the experimental protocols presented herein do not always result in reproducible amounts of capping OA in Q-PbS.

The presence of OA and ODE does not distort the interpretation of QD voltammograms. Indeed, in auxiliary experiments, OA or ODE were deposited onto the working electrode and the potential was swept likewise in the QD experiments. No peak currents but only rising anodic and cathodic currents commencing at $E > 0.0$ and < -0.8 V were registered, respectively.

In the final part of the paper, we present experimental data for QD-100SH. This sample as well as QD-60SH demonstrates stable electrochemical response without notable oxidation A1 and with intensive (apparently irreversible) oxidation and reduction processes, A2 and C3, at the extremes of potential window (fig. 9).

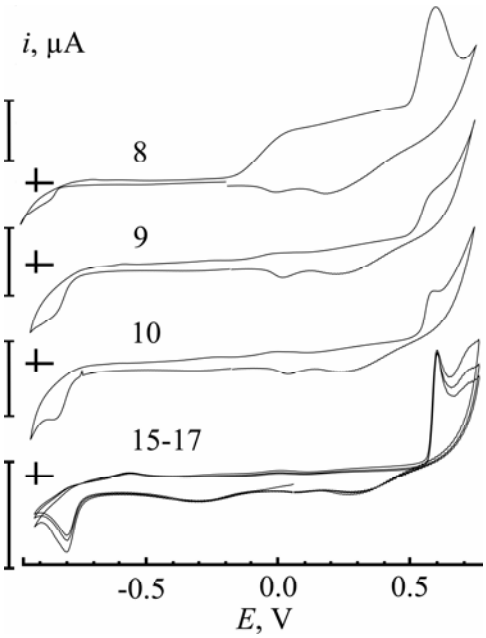

Fig. 9. Cyclic voltammograms of sample QD-100SH. Numbers show the cycle number. The bars are all 50 μA. Scan direction: OCP → -0.9 → 0.75 → OCP

As mentioned before, we associate process C3 with PbS reduction. The nature of process A2 remains mostly unknown. Both processes are formed after prolonged potential cycling in the interval -0.9 – 0.75 V. Specifically, after 7 consecutive cycles, the working electrode with the QDs was taken out of the cell, washed with water, acetone, dried in Ar stream and inserted in the cell again. The following cycles 8–10 and 15–17 are shown in the same figure. As is evident, virtually identical *i-E* profiles are produced at cycles

15–17. Further experiments revealed that washing and drying the working electrode is not important in obtaining a stable response; suffice to leave the electrode in the solution for some time and then resume potential cycling. Apparently some soluble reaction products are gradually removed from the electrode surface during the time of rest.

The stability of voltammograms allowed us to extract quantitative information from peak currents, i_{max}, as well as peak potentials, E_{max}, for a single deposition. Firstly, i_{max} values show an irregular trend to increase at faster scan rates, if potential is cycled in the range -0.9 – 0.75 V. However, i_{max} demonstrates linear dependency on the scan rate, s, if potential cycling is confined within the range -0.3 – 0.85 V (see fig. 10,*a* and *b*). A reversible depolarization of absorbed species results in such a dependency and the potentiodynamic curve represents a symmetrical bell-shape profile, as is generally known [56, 57]. Obviously, the reaction in question is not reversible. It can be shown that irreversible and quasi-reversible depolarization of adsorbed species gives the same result. The theory of these electrochemical reactions complying with the Butler-Volmer kinetics was first presented by Hubbard [58]. Besides the peak currents given by formula (12), the shift of the peak potential with the scan rate given by formula (13)* also brings important information and can be used to verify the compliance of the irreversible model, Red - ne → Ox, with the data.

$$i_{max} = \frac{(1-\alpha)n_0 F}{2.71RT} nF[\mathrm{Red}]_0 s \tag{12}$$

$$E_{max} = E^{0'} + \frac{2.303RT}{(1-\alpha)n_0 F} \lg\left[\frac{(1-\alpha)n_0 Fs}{k_0 RT}\right] \tag{13}$$

where α is the transfer coefficient from the Butler-Volmer equation, n_0 is the number of electrons transferred in an elementary step, n is the number of electrons transferred in an overall reaction, F is the Faraday constant, k_0 is the oxidation reaction rate coefficient independent on the potential, $[\mathrm{Red}]_0$ is the initial amount of reductant (mole) adsorbed on the electrode surface, s is the scan rate (V/s), R is universal gas constant.

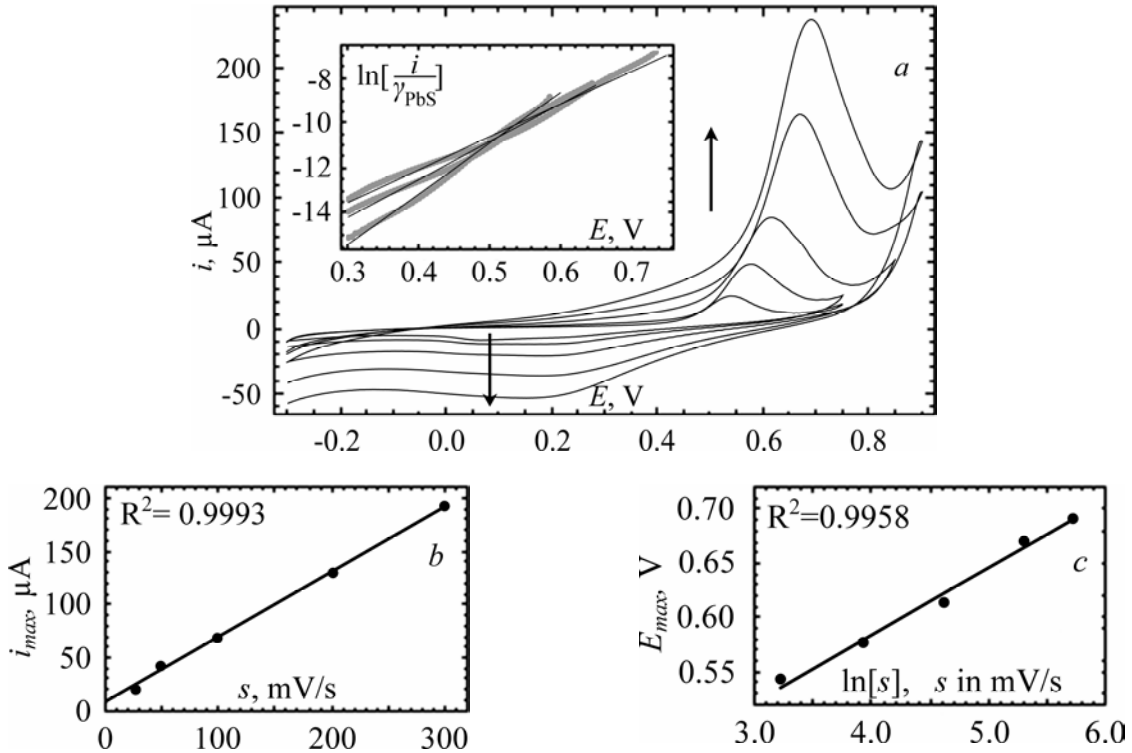

Fig. 10. Cyclic voltammograms of sample QD-100SH at scan rates 25, 50, 100, 200 and 300 mV/s with the potential sweep -0.3 → (0.75-0.9) → -0.3 V. The inset demonstrates the linearization of peak A2 for scan rates 25, 100 and 300 mV/s. The arrows point the change in voltammograms with increasing scan rate (a). Peak current as a function of the scan rate (b) and peak potential as a function of logarithm of the scan rate (c) based on the data shown in (a)

*Formula (13) also deduced by the authors differs from the one given in [58] by the ratio V/A omitted under logarithm function since Hubbard considered thin layer cells electrochemistry.

According to (13), the plot of E_{max} vs lg[s] contains the reciprocal of the Tafel constant, $\frac{(1-\alpha)n_0F}{RT}$, and the interception presents a linear relationship between $E^{0\prime}$ and ln[k_0] thereby the two quantities cannot be determined from this experiment. Our data yield a straight line in the coordinates (fig. 10,*c*) and the Tafel constant of 16.18 or 142 mV/decade and $(1-\alpha)n_0 = 0.42$. On the other hand, the Tafel slope might be estimated from (12). Indeed, plotting i_{max} vs s gives a straight line with the slope of 0.610 (fig. 10,*b*). However, the slope includes the product $nF[\text{Red}]_0$ which is the peak charge, q_{A2}. Unfortunately, peak A2 cannot be reliably separated from the other signal following it and, therefore, the peak charge is unavailable. Inversely, q_{A2} can be estimated from that slope if the Tafel constant is known; simple calculation gives $q_{A2} = 102$ μC. This value agrees with the expected one for the irreversible model. The charge values of peak A2 before E_{max} are reproducible at various scan rates and vary between 58 and 61 μC. Since *i-E* profile of an irreversible reaction is asymmetric, with most of the charge passed before the peak potential, q_{A2} must be << 120 μC, which is in agreement with the anticipated peak shape. This value is used further to obtain the Tafel constant from linearization of the potentiodynamic curves A2. Indeed, the plot of lg[i/γ_{Red}] vs E yields a fairly good linear dependency (the inset in fig. 10,*a*) but the slopes (the Tafel constants) diminish with the scan rate (see table 3). This contradicts a little the result just mentioned. Namely, the Tafel constant found according to (13) has a certain value and one would expect the same value from the linearization. The mean value for the slopes obtained from the linearization amounts to 134 mV/decade, which is rather close to the value found from (13). Apparently, formula (13) yields an averaged Tafel constant that, in fact, varies in the experiments performed at different scan rates. We are convinced that process A2 is more complex than a one-stage irreversible oxidation reaction and the regularities found experimentally are covered by this model only in part. Besides, the process can be complicated by diffusion especially at earlier stages.

Table 3. The data on the linearization of peak A2 for QD-100SH for different scan rates

scan rate, mV/s	intercept	slope	slope, mV/decade	R^2
25	-22.08	9.71	103	0.9952
50	-20.75	8.49	118	0.9749
100	-19.15	7.23	138	0.9892
200	-18.55	6.65	150	0.9849
300	-17.84	6.28	159	0.9858

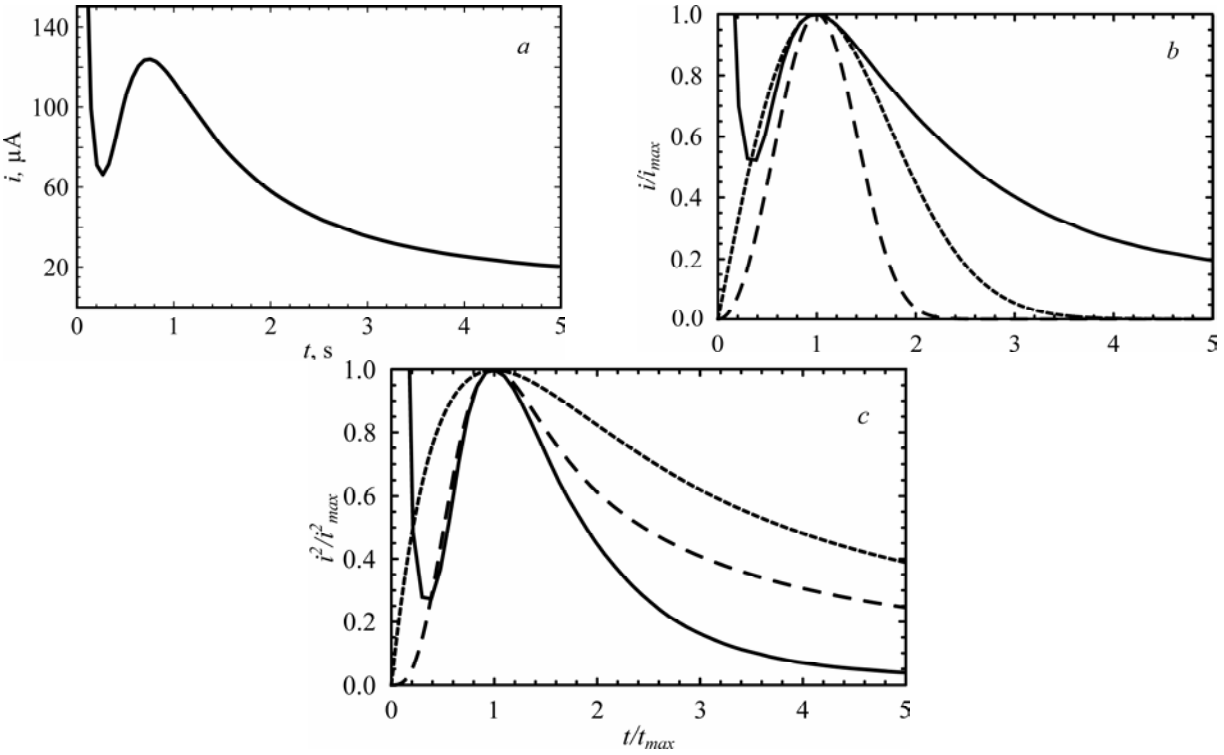

Fig. 11. Potential step experiment: from E_1 = OCP (~0.0 V) to E_2 = 0.65 V (a). The plots of the data from (a) in dimensionless coordinates (——), constructed according to instantaneous (----) and progressive (– – –) growth models in the case of 2D (b) and 3D (c) deposits

Chronoamperometry experiments revealed the formation of a new phase in the A2 region. The potential was stepped from OCP (~0.0 V) to 0.65 V, giving a characteristic curve, $i(t)$, with a maximum (fig. 11,*a*). It is not possible to determine which type of nucleation operates in this case. The dimentionless plot of i/i_{max} vs t/t_{max} for the experimental data, given in fig. 11,*b* and *c*, is not adequate at higher times with any of the four models of progressive (2D, 3D) or instantaneous (2D, 3D) nucleation [59–61]. Probably, a passive film grows on the QD surface and bulk PbS thin films beyond a monolayer coverage (2D) but blocking the surface prevents further 3D growth.

An attempt to investigate an oxidation process of galena at far anodic potentials (apparently A2) at pH = 12 was also made in [52]. The nature of chemical reactions involved remained unclear. The authors only suggested that passivating film that had formed at earlier stages of galena oxidation dissolved and another one formed.

As is obvious, the electrochemistry of PbS is very complex and probably only spectroscopic and chemical analyses of PbS electrode surface during or after a potential sweep may shed light on the chemistry of the reactions involved.

CONCLUSIONS

1. The synthesized Q-PbS showed PL maxima in the range 800–1300 nm, indicating a quantum confinement effect; the radius of nanocrystals was estimated to vary between 4–8 nm.

2. By means of IR spectroscopy, the OA molecules were found to face the nanocrystal surface with their carboxyl groups, forming a surface compound – lead oleate. Refluxing Q-PbS in acetone or heating it with NaOH, being a purification procedure, resulted in a partial removal of OA from the synthesized product. The purification improved voltammetric response of Q-PbS.

3. Cyclic voltammograms of Q-PbS deposited onto a working electrode essentially followed that of bulk PbS thin films obtained by chemical bath deposition. The slight cathodic shift of the oxidation peak is accounted for by the change in the formal potential of the oxidation reaction. The oxidation and reduction of Q-PbS are governed solely by the thermodynamics of the respective redox reactions, and electronic structure of those QDs is not manifested, as follows from the experimental data. A simple explanation of PbS reduction and oxidation is formulated from the viewpoint of electrochemistry of semiconductors.

4. The peculiarities of Q-PbS electrochemistry consisted in *a*) the ability of Q-PbS to participate in multiple redox cycles whereas bulk PbS films dissolved fast upon oxidation, *b*) the layer-by-layer oxidative dissolution that was manifested as reproducibility of peak currents and charges between various experiments, and *c*) stabilizing voltammetric response after multiple redox cycles. The presence of capping OA layers which prevent the redox products from escaping in the solution bulk is suggested to account for these effects.

5. Kinetics of two oxidation peaks A1 and A2 was investigated by the linearization of potentiodynamic curves, suggested in the present study. Kinetics of process A1 for bulk PbS films is consistent with the dissolution of a binary ionic semiconductor; the transfer coefficient was determined $\alpha_{Pb}^{+} = 0.52$. Process A1 for the QDs turned out to be more complex: the linearization was not as effective as it was for bulk PbS. The oxidation occurs slightly faster. The chemical nature of process A2 remained unclear. Our data only suggested the involvement of adsorbed species and the growth of a new phase.

ACKNOWLEDGEMENTS

We are thankful to our colleagues Maria Rusu and Diana Shepel from the Institute of Chemistry of the Academy of Sciences of Moldova for FT-IR measurements. This work was supported by the state grants in the framework of institutional projects of the Institute of Applied Physics of the Academy of Sciences of Moldova 11.817.05.03A and 11.817.05.05A.

APPENDIX

Normally the Tafel constants are not extracted from potentiodynamic curves due to the involvement of diffusion of redox species. Here we show that the Tafel constants can be obtained from a single potentiodynamic curve if 1) the redox species are pre-adsorbed onto an electrode surface, 2) they do not continue to adsorb from or diffuse away into the solution during the sweep of potential, 3) the electron transfer reaction is irreversible, 4) no chemical reactions precede the electron transfer and 5) the redox reaction follows the Butler-Volmer kinetics. Then one can write the Butler-Volmer equation [62] for the oxidation reaction $\mathrm{Red} - ne \rightarrow \mathrm{Ox}$ with the constant of backward reaction, $k_b = 0$, as follows:

$$i = k_0 nF[\mathrm{Red}]\exp\left[\frac{(1-\alpha)nF}{RT}\left(E - E^{0'}\right)\right]. \qquad \text{(A1)}$$

If we denote relative amount of the reductant as

$$[\mathrm{Red}]/[\mathrm{Red}]_0 = \gamma_{\mathrm{Red}} \tag{A2}$$

where $[\mathrm{Red}]_0$ is the initial amount of Red, then γ_{Red} can be found from experimental data as follows:

$$\gamma_{\mathrm{Red}} = 1 - [\mathrm{Ox}]/[\mathrm{Ox}]_\infty = 1 - q/q_{tot} \tag{A3}$$

where $[\mathrm{Ox}]_\infty$ is the final amount of the oxidant, q is the peak charge at any instant and q_{tot} is the charge under the whole peak corresponding to the redox reaction considered. Using and the total charge expressed as $q_{tot} = nF[\mathrm{Red}]_0$, can be re-written

$$\frac{i}{\gamma_{\mathrm{Red}}} = k_0 q_{tot} \exp\left[\frac{(1-\alpha)nF}{RT}\left(E - E^{0'}\right)\right]. \tag{A4}$$

Plotting $\ln\left[\frac{i}{\gamma_{\mathrm{Red}}}\right]$ vs potential E results in a straight line with the slope being a Tafel constant and the interception as given below:

$$\text{slope} = \frac{(1-\alpha)nF}{RT} \tag{A5}$$

$$\text{interception} = \ln\left[k_0 q_{tot}\right] - \text{slope}\ E^{0'} \tag{A6}$$

If one knows $E^{0\prime}$ then k_0 can be determined from a single experiment. The approach presented holds if the redox process follows the Tafel-like kinetics as is the case of the dissolution of an ionic semiconductor, according to (A5) and (A6); but the slope and the intercept have a different interpretation.

REFERENCES

1. Wise F.W. Lead Salt Quantum Dots: the Limit of Strong Quantum Confinement. *Acc. Chem. Res.*, 2000, **33**(11), 773–780.
2. Vasilyeva E., Lam B., Fang Zh., Minden M.D., Sargent E.H., Kelley S.O. Direct Genetic Analysis of Ten Cancer Cells: Tuning Sensor Structure and Molecular Probe Design for Efficient mRNA Capture. *Angew. Chem. Int. Edit*. 2011, **50**(18), 4137–4141.
3. Talapin D.V., Lee J.S., Kovalenko M.V., Shevchenko E.V. Prospects of Colloidal Nanocrystals for Electronic and Optoelectronic Applications. *Chem. Rev.*, 2009, **110**(1), 389–458.
4. Konstantatos G., Howard I., Fischer A., Hoogland S., Clifford J., Klem E., Levina L., Sargent E.H. Ultrasensitive Solution-cast Quantum dot Photodetectors. *Nature*, 2006. **442**(7099), 180–183.
5. McDonald S.A., Konstantatos G., Zhang Sh., Cyr P.W., Klem E. J.D., Levina L., Sargent E.H. Solution-processed PbS Quantum Dot Infrared Photodetectors and Photovoltaics. *Nature Materials*, 2005, **4**(2), 138–142.
6. Jiang X.M., Schaller R.D., Lee S.B., Pietryga J.M., Klimov V.I., Zakhidov A.A. PbSe Nanocrystal/Conducting Polymer Solar Cells with an Infrared Response to 2 Micron. *J. of Mater. Res.*, 2007, **22**(8), 2204–2210.
7. Kamat P.V., Tvrdy K., Baker D.R., Radich J.G. Beyond Photovoltaics: Semiconductor Nanoarchitectures for Liquid-Junction Solar Cells. *Chem. Rev.*, 2010, **110**(11), 6664–6688.
8. Schaller R.D., Petruska M.A., Klimov V.I. Effect of Electronic Structure on Carrier Multiplication Efficiency: Comparative Study of PbSe and CdSe Nanocrystals. *Appl. Phys. Lett*., 2005, **87**(253102).
9. Steckel J.S., Coe-Sullivan S., Bulović V., Bawendi M.G. 1.3 μm to 1.55 μm Tunable Electroluminescence from PbS Quantum Dots Embedded within an Organic Device. *Adv. Mater.*, 2003. **15**(21), 1862–1866.
10. Kucur E., Bücking W., Nann T. Electrochemical Determination of Mesoscopic Phenomena, Defect States in CdSe Nanocrystals and Charge Carrier Manipulability. *Microch. Acta*, 2008, **160**(3), 299–308.
11. Bard A.J., Ding Zh., Myung N. Electrochemistry and Electrogenerated Chemiluminescence of Semiconductor Nanocrystals in Solutions and Films. *Struct. Bond.*, 2005, **118**, 1–57.
12. Archer M.D., Nozik A.J. *Nanostructured and Photoelectrochemical systems for Solar Photon Conversion*, vol. 3. 2008. London: Imperial College Press. 760 p.

13. Hyun B.-R., Yu-Wu.Zhong Y.-W., Bartnik A.C., Sun L., Abruna H.D., Wise F.W., Goodreau J.D., Matthews J.R., Leslie T.M., Borrell N.F. Electron Injection from Colloidal PbS Quantum Dots into Titanium Dioxide Nanoparticles. *ACS Nano*, 2008, **2**(11), 2206–2212.
14. Sato N. *Electrochemistry at Metal and Semiconductor Electrodes.* Amsterdam: Elsevier Science B.V. 1998. 400 p.
15. Haram S.K., Quinn B.M., Bard A.J. Electrochemistry of CdS Nanoparticles: A Correlation between Optical and Electrochemical Band Gaps. *J. Am. Chem. Soc.*, 2001, **123**(36), 8860–8861.
16. Kucur E., Riegler J., Urban G.A., Nann T. Determination of Quantum Confinement in CdSe Nanocrystals by Cyclic Voltammetry. *J. Chem. Phys.*, 2003, **119**(4), 2333–2337.
17. Gaponik N., Poznyak S.K., Osipovich N.P., Shavel A., Eychmüller A. Electrochemical Probing of Thiol-Based Nanocrystals. *Microchim. Acta*, 2008, **160**(3), 327–334.
18. Inamdar S.N., Ingole P.P., Haram S.K. Determination of Band Structure Parameters and the Quasi-Particle Gap of CdSe Quantum Dots by Cyclic Voltammetry. *Chem. Phys. Chem.*, 2008, **9**(17), 2574–2579.
19. Dissanayake D.M.N.M., Lutz T., Curry R.J., Silva S.R.P. Measurement and Validation pf PbS Nanocrystal Energy Levels, *Appl. Phys. Lett.*, 2008, **93**(043501).
20. Guyot-Sionnest P. Charging Colloidal Quantum Dots by Electrochemistry. *Microchim. Acta*, 2008, **160**(3), 309–314.
21. Wehrenberg B.L., Guyot-Sionnest P. Electron and Hole Injection in PbSe Quantum Dot Films. *J.Am. Chem. Soc.*, 2003, **125**(26), 7806–7807.
22. Talgorn E., Moysidou E., Abellon R.D., Savenije T.J., Goossens A., Houtepen A.J., Siebbeles L.D.A. Highly Photoconductive CdSe Quantum-Dot Films: Influence of Capping Molecules and Film Preparation Procedure. *J. Phys. Chem. C*, 2010, **114**(8), 3441–3447.
23. Greene I.A., Wu F., Zhang J.Z., Chen S. Electronic Conductivity of Semiconductor Nanoparticle Monolayers at the Air/Water Interface. *J. Phys. Chem.*, 2003, **107**(24), 5733–5739.
24. Ogawa Sh., Hu K., Fan F.-R. F., Bard A.J. Photoelectrochemistry of Films of Quantum Size Lead Sulfide Particles Incorporated in Self-Assembled Monolayers on Gold. *J. Phys. Chem. B*, 1997, **101**(29), 5707–5711.
25. Sun L., Lei B., Hyun B.-R., Bartnik A.C., Zhong Y.-W., Reed C.J., Pang D.-W., Abruna H.D., Malliaras G.G., Wise F.W. Electrogenerated Chemiluminescence from PbS Quantum Dots. *Nano Letters*, 2009, **9**(2), 789–793.
26. Chen S., Traux L.A., Sommers J.M. Alkanethiolate-Protected PbS Nanoclusters: Synthesis, Spectroscopic and Electrochemical Studies. *Chem. Mater.*, 2000, **12**(12), 3864–3870.
27. Hines M.A., Scholes G.D. Colloidal PbS Nanocrystals with Size-Tunable Near-Infrared Emission: Observation of Post-Synthesis Narrowing of the Particle Size Distribution. *Adv. Mater.*, 2003, **15**(21), 1844–1849.
28. Belova N.S., Uritskaya A.A., Kitaev G.A. Kinetics of Lead Sulphide Precipitation from Citrate Solutions of Thiourea. *Russian Journal of Applied Chemistry*, 2002, **75**(10), 1562–1565.
29. Patil R.S., Pathan H.M., Gujar T.P., Lokhande C.D. Characterization of Chemically Deposited PbS Thin Films. *J. Mater. Sci.*, 2006, **41**(17), 5723–5725.
30. Rempel A.A., Kozhevnikova N.S., Leenaers A.J.G., Berghe S. Towards Particle Size Regulation of Chemically Deposited Lead Sulfide (PbS). *J. Cryst. Growth*, 2005, **280**(1-2), 300–308.
31. Rodriguez J.M.D., Melian J.A.H., Pena J.P. Determination of the Real Surface Area of Pt Electrodes by Hydrogen Adsorption Using Cyclic Voltammetry. *J. Chem. Edu.*, 2000, **77**(9), 1195–1197.
32. Angerstein-Kozlowska H., Conway B.E., Sharp W.B.A. The Real Condition of Electrochemically Oxidized Platinum Surfaces. Part I. Resolution of Component Processes. *Journal of Electroanalytical Chemistry and Interfacial Electrochemistry*, 1973, **43**(1), 9–36.
33. Gaponenko S.V. *Optical properties of semiconductor nanocrystals*. Cambridge: Cambridge University Press. 1998. 260 p.
34. Wang Y., Suna A., Mahler W., Kasowski R. PbS in Polymers. From molecules to bulk solids. *J. Chem. Phys.* 1987, **87**(12), 7315–7322.
35. Sole J.G., Bausa L.E., Jaque D. *An Introduction to the Optical Spectroscopy of Inorganic Solids*. 2005. Chechister: John Wiley and Sons. 283 p.
36. Butler I.B., Schoonen M.A.A., Rickard D.T. Removal of Dissolved Oxygen from Water: A Comparison of Four Common Techniques. *Talanta*, 1994, **41**(2), 211–215.
37. Richardson P.E., O'Dell C.S. Semiconducting Characteristics of Galena Electrodes. *Journal of Electrochemical Society: Electrochemical Science and Technology*, 1985, **132**(6), 350–356.
38. Smith A.L. *Applied Infrared Spectroscopy: Fundamentals, Techniques and Analytical Problem-Solving*. New York: John Wiley and Sons, Inc. 1979. 327 p.

39. Lobo A., Möller T., Nagel M., Borchert H., Hickey S.G., Weller H. Photoelectron Spectroscopic Investigation of Chemical Bonding in Organically Stabilized PbS Nanocrystals. *J. Phys. Chem. B*, 2005, **109**(37), 17422–17428.
40. Janietz S., Bradley D.D.C., Grell M., Giebeler S., Inbasekaran M., Woo E.P. Electrochemical Determination of the Ionization Potential and Electron Affinity of poly(9,9-dioctylfluorene). *Appl. Phys. Lett.*, 1998, **73**(17), 2453–2455.
41. Sommer M., Lindner S.M., Thelakkat M. Microphase-Separated Donor-Acceptor Diblock Copolymers: Influence of Homo Energy Levels and Morphology on Polymer Sollar Cells. *Adv. Funct. Mater.*, 2007, **17**(9), 1493–1500.
42. Colladet K., Nicolas M., Goris L., Lutsen L., Vanderzande D. Low-Band Gap Polymers for Photovoltaic Applications. *Thin Solid Films*, 2004, **451-452**, 7–11**.**
43. Wan J.-H., Feng J.-C., Wen G.-A., Wang H.-Y., Fan Q.-L., Wei W., Huang C.-H., Huamg W. New p–n Diblock and Triblock Oligomers: Effective Tuning of HOMO/LUMO Energy Levels. *Tetrahedron Lett.*, 2006, **47**(16), 2829–2833.
44. Brunner K., Dijken A., Börner H., Bastiaansen J., Kiggen N.M.M., Langeveld B.M.W. Carbazole Compounds as Host Materials for Triplet Emitters in Organic Light-Emitting Diodes: Tuning the HOMO Level without Influencing the Triplet Energy in Small Molecules. *J. Am. Chem. Soc.*, 2004, **126**(19), 6035–6042.
45. Lai R.Y., Fleming J.J., Merner B.L., Vermeij R.J., Bodwell G.J., Bard A.J. Photophysical, Electrochemical, and Electrogenerated Chemiluminescent Studies of Selected Nonplanar Pyrenophanes. *J. Phys. Chem. A*, 2004, **108**(3), 376–383.
46. Loukova G.V. The First Experimental Approach to Probing Frontier Orbitals and HOMO-LUMO Gap in Bent Meatllocenes. *Chem. Phys. Lett.*, 2002, **353**(3-4), 244–252.
47. Xia S.J., Birss V.I. In situ Mass and Ellipsometric Study of Hydrous Oxide Film Growth on Pt in Alkaline Solutions. *Electrochim. Acta*, 2000, **45**(22-23), 3659–3673.
48. Gardener J.R., Woods R. A Study of the Surface Oxidation of Galena Using Cyclic Voltammetry. *J. Electroanal. Chem.*, 1979, **100**(1-2), 447–459.
49. Nicol M.J., Paul R.L., Diggle J.W. The Electrochemical Behaviour of Galena (Lead Sulphide) – II. Cathodic Reduction. *Electrochim. Acta*, 1978, **23**, 635–639.
50. Гладышев В.П., Киреева Е.П. Восстановление свинца из взвеси галенита (PbS) на ртутном электроде. *Электрохимия*, 1972, **7**(7), 977–981.
51. Saloniemi H., Kemell M., Ritala M., Leskelä M. Electrochemical Quartz Crystal Microbalance Study on Cyclic Electrodeposition of PbS thin-films. *Thin Solid Films*, 2001, **386**(1), 32–40.
52. Paul R.L., Nicol M.J., Diggle J.W., Sauders A.P. The Electrochemical Behaviour of Galena (Lead Sulphide) – I. Anodic Dissolution. *Electrochim. Acta*, 1978, **23**, 625–633.
53. Crundwell F.K. The Influence of the Electronic Structure of Solids on the Anodic Dissolution and Leaching of Semiconducting Sulphide Minerals. *Hydrometallurgy*, 1998, **21**(2), 155–190.
54. Pleskov Yu.V., Gurevich Yu.Ya. "Electrochemistry of Semiconductors: New Problems and Prospects" in *Modern Aspects of Electrochemistry*. No. 16. Ed. Conway B.E., White R.E, Bockris J.O'M. 1985. New York: Plenum Press.
55. Scharifker B., Ferreira Z., Mozota J. Electrodeposition of Lead Sulphide. *Electrochim. Acta*, 1985, **30**(5), 677–682.
56. Brett C.M.A., Brett A.M.O. *Electrochemistry: Principles, Methods, and Applications.* 1994. New York: Oxford University Press. 427 p.
57. Scholz F. *Electroanalytical Methods: Guide to Experiments and Applications*. 2002. New York: Springer. 331 p.
58. Hubbard A.T. Study of the Kinetics of Electrochemical Reactions by Thin-Layer Voltammetry: I. Theory. *Electroanalytical Chemistry and Interfacial Electrochemistry*, 1969, **22**(2), 165–174.
59. Scharifker B., Mostany J. Three-Dimensional Nucleation with Diffusion Controled Growth. Part I. Number Density of Active Sites and Nucleation Rates per Site. *J. Electroanal. Chem.*, 1984, **177**(1-2), 13–23.
60. Scharifker B., Hills G. Theoretical and Experimental Studies of Multiple Nucleation. *Electrochim. Acta*, 1983, **28**(7), 879–889.
61. Bade K., Tsakova V., Schultze J.W. Nucleation, Growth and Branching of Polyaniline from Microelectrode Experiments. *Electrochim. Acta*, 1992, **37**(12), 2255–2261.
62. Calvo E.J. "The Current-Potential Relationship" in *Encyclopaedia of Electrochemistry: Interfacial kinetics and mass transport* (vol. 2). Ed. Bard A.J. 2003. New-York: Wiley-VCH. 553 p.

Received 02.08.11

Реферат

В работе методами циклической вольтаметрии (ЦВ) и хроноамперометрии исследуется электрохимический отклик квантовых точек (КТ) PbS, покрытых слоем олеиновой кислоты (ОК) и осажденных на платиновый электрод, в водном 0,1 М NaOH. КТ также были охарактеризованы при помощи инфракрасной и фотолюминесцентной спектроскопии. Интерпретация данных циклической вольтаметрии КТ проводится на основе сравнительного анализа результатов вольтаметрии тонких пленок массивного PbS, полученных методом химического осаждения из раствора. Было установлено, что оба материала дают очень схожие вольтамограммы, однако, окисление КТ, как правило, начинается при более отрицательных потенциалах, чем у массивного материала. Это объясняется влиянием покрывающих слоев ОК, в которых молекулы ОК реагируют с Pb^{2+}, образуя трудно-растворимый олеат свинца, смещая, таким образом, формальный редокс-потенциал в катодную область. Методы, позволяющие удалить часть ОК из КТ, приводят к анодному смещению потенциала окисления в область, характерную для массивного материала. Обсуждается возможность определения абсолютных положений дна зоны проводимости и потолка валентной зоны в КТ методом ЦВ; однако, взаимосвязь вольтамметрии КТ и их электронной структуры экспериментально не обнаружена. КТ PbS способны выдержать множество циклов окисления-восстановления в то время как массивный материал легко растворяется при первом окислении. Этот эффект объясняется наличием слоев ОК, которые препятствуют диффузии растворимых продуктов окисления в раствор. Некоторые образцы КТ PbS демонстрировали особую стабильность к окислению, характерному для PbS и начинающемуся при -0,2 В по Ag/AgCl (нас.), и стабильный сигнал окисления и восстановления при более высоких (0,55 В) и более низких (-0,8 В) потенциалах, соответственно.
